Composite Structures 321 (2023) 117228

Contents lists available at ScienceDirect

Composite Structures

journal homepage: www.elsevier.com/locate/compstruct

Temperature dependence analysis of mechanical properties and bending behaviors of shape memory programmable composites

Zhengxian Liu [a], Xin Lan [a], Chengjun Zeng [b], Liwu Liu [b], Wenfeng Bian [c], Jinsong Leng [a], Yanju Liu [b,*]

[a] Centre for Composite Materials and Structures, Harbin Institute of Technology (HIT), Harbin 150080, People's Republic of China
[b] Department of Astronautical Science and Mechanics, Harbin Institute of Technology (HIT), Harbin 150001, People's Republic of China
[c] Department of Civil Engineering, Harbin Institute of Technology (HIT), Weihai 264209, People's Republic of China

ARTICLE INFO

Keywords:
Shape memory polymer composites
Temperature dependence
Buckling behavior
Mechanical properties

ABSTRACT

Temperature significantly affects the mechanical properties of shape memory polymers (SMPs). The temperature dependence of mechanical properties and bending behaviors of shape memory polymer composites (SMPCs) was investigated in this study. Dynamic mechanical analysis and static mechanical tests were performed to investigate the temperature dependence on the mechanical properties of SMP and SMPC. The tensile strength and shear strength of SMP declined as the temperature rose, while the elongation at break increased first and subsequently reduced. SMPC exhibited brittle fracture at low temperatures and fiber buckling at high temperatures, respectively. Subsequently, a temperature-dependent model of the bending behavior of SMPC was developed. Theoretical model revealed the effect of temperature and fiber volume content on fiber buckling. The higher the temperature and fiber volume content is, the easier the fiber buckles. The effects of temperature, thickness and fiber volume content on critical buckling curvature, strain energy, half-wavelength and amplitude were investigated. Temperature and fiber volume content were positively related to critical buckling curvature, strain energy and amplitude, but negatively related to half-wavelength. Thickness was positively related to strain energy, half-wavelength and amplitude, but negatively correlated to critical buckling curvature, in which thickness does not determine whether SMPC buckling occurs. Eventually, the theoretical model was verified using the four-point bending test to ensure its credibility. The research results are expected to provide theoretical guidance for the design and application of SMPC.

1. Introduction

Shape memory polymers (SMPs) are a novel type of multifunctional materials that can sense the changes in the external environment and respond actively [1–4], with thermal, light, electricity, magnetism, and solution as driving modalities [5–7]. The thermal drive is the most basic and widely used direct drive mode [8]. When the temperature falls below the glass transition temperature (Tg) of SMP, the internal molecular chain freezes, and the modulus of SMP increases. When the temperature rises above Tg, the internal molecular chain gradually thaws and the modulus decreases, allowing it to be programmed into a temporary shape under external force [9,10]. When the temperature drops below Tg, the modulus of SMP recovers to its initial level. The modulus of SMP and temperature have a one-to-one relationship, and SMP exhibits variable stiffness properties [11].

Shape memory programmable composites have the potential to significantly enhance the reliability, stability, and environmental adaptability of SMPs, while also expanding their application scenarios. The addition of reinforcement to SMPs can effectively improve their mechanical properties while maintaining their shape memory effect [12,13]. Generally, long fibers, short fibers, and particles are added as reinforcing phases to form shape memory polymer composites (SMPCs). SMPCs exhibit advantages such as high specific strength, high specific stiffness, low impact unfolding, and repeatable programming, making them suitable for various fields, such as aviation, aerospace, and medical applications [14]. Long fibers outperform particles and short fibers in terms of heat conductivity, strength, and recovery force [15,16]. Additionally, long fiber reinforced SMPC can also achieve a high packaging ratio. The buckling deformation of the internal fiber during bending is the primary mechanism [17]. As a result, long fiber reinforced SMPC is

* Corresponding author.
E-mail address: yj_liu@hit.edu.cn (Y. Liu).

https://doi.org/10.1016/j.compstruct.2023.117228
Received 9 December 2022; Received in revised form 14 April 2023; Accepted 3 June 2023
Available online 4 June 2023

commonly employed in space deployable structures [14,18].

The temperature-dependent properties of SMP material have also attracted the attention of researchers [19,20]. Yin *et al* [21] developed an improved thermo-viscoelastic finite deformation constitutive model to predict the constraint recovery behavior and stress–strain response of particle-reinforced SMPC at different temperatures, providing an effective method for the design and optimization of particle reinforced SMPC. Bhola *et al* [22] established a theoretical and numerical framework to describe the thermo-mechanical deformation response of SMPC laminates. The model can predict the significant characteristics such as shape fixation, recovery, and rebound response. Li *et al* [23] established a logarithmic rate-based viscoelastic-viscoplastic model to describe the shape memory behavior of temperature hysteresis, and gave temperature dependent equations for material parameters. Leng *et al* [24] established a prediction model for the elastic constants of fiber-reinforced SMPC in the temperature range of 20 ~ 120 °C. The prediction model accurately described the elastic constants of laminated plates changing with temperature. However, there are few studies on how temperature affects the buckling behavior of SMPC during bending. SMPC exhibits strong temperature sensitivity. Therefore, the motivation of this study is to comprehensively investigate the influence of temperature on the mechanical properties and bending behaviors of SMPC. This work provides a simple and convenient model for predicting the temperature-dependent bending behavior of SMPC, which can serve as a valuable reference for the design, optimization, and analysis of SMPC in practical applications. This study has positive significance for promoting the development of the SMPC field.

In this study, temperature dependence of mechanical properties of SMPC were investigated. The mechanical properties of SMP were systematically characterized to comprehend the influence of temperature on SMP properties. The temperature dependence of SMPC bending behavior was studied theoretically on the basis of collecting the fundamental material properties. The effects of temperature and fiber volume content on the micro buckling of SMPC were studied by phase transition model and critical buckling analysis. The total strain energy of the SMPC micro-bucking system was developed. The minimum energy principle was used to predict how temperature, thickness, and fiber volume content affect the curvature, strain energy, half-wavelength, and amplitude of critical buckling. The study found that SMPC exhibited brittle fracture at low temperatures and fiber buckling at high temperatures, respectively. The higher the temperature and fiber volume content is, the easier the fiber buckles.

2. Experimental

In this study, to theoretically investigate the temperature dependence of SMPC, the mechanical properties of pure SMP were first tested to study the temperature dependence of its mechanical properties. Then, material analysis was provided as a basis for the temperature dependence analysis of composite.

2.1. Material preparation

The matrix used in this study is a shape memory epoxy resin developed by Jinsong Leng's Research Group [25]. The curing temperature is set at 80 °C and 100 °C for 3 h each, followed by 150 °C for 5 h, with a temperature transition time of 30 min. The unidirectional fiber reinforced SMPC was prepared using prepreg technology, and the fiber volume content was controlled at 30.08% by adjusting the thickness of the prepreg and the adhesive film. A low-modulus carbon fiber with a tensile modulus of 45 GPa, an elongation at break of 2.4%, and a single diameter of 8 mm, provided by Guangwei Composite Materials Co., Ltd, was used in this study. Previous research has demonstrated that SMPC with a low modulus can achieve a high packaging ratio in engineering applications [26].

2.2. Dynamic mechanical analysis

The dynamic thermal–mechanical properties of SMP and SMPC were characterized using a dynamic mechanical analyzer (DMA, Q800, TA Instruments, New Castle, USA). The force range of the equipment was 0.001 ~ 18 N, and the temperature range was −150 ~ 500 °C. The pure polymer was tested in the tensile mode with a specimen dimension of 60 mm × 3 mm × 1.5 mm. The loading frequency was set at 2 Hz, and the temperature range was 25 ~ 170 °C, with a heating rate of 2 °C/min.

2.3. Tensile and shear test of SMP

Tensile and shear tests were conducted to investigate the impact of temperature on the static mechanical properties of SMP. The static tensile test of SMP was performed using a universal material testing machine (Z-wick Z010) in accordance with the ASTM-D638 Type IV standard. The machine was equipped with a temperature chamber (-50 ~ 300 °C) and an automated large deformation optical extensometer, which provided a precise tensile strain and temperature environment. The tensile rate was 2 mm/min. The shear properties of SMP were evaluated using a punch tool, and the shear test was performed in accordance with ASTM-D732. The shear specimen's dimensions were Φ50 mm × 1.5 mm, and the center hole diameter was 11 mm. The test rate was 1 mm/min, and the temperatures were 25 °C, 60 °C, 90 °C, 120 °C, and 150 °C, respectively. The number of effective test specimens for all tests was not less than 5.

2.4. Bending test of SMPC

The bending performance of SMPC was characterized at various temperatures using the guidance of standard ASTM-D7264. Bending tests were conducted on specimens with dimensions of 60 mm × 12.7 mm × 1.5 mm, an effective span of 32 mm, and a loading rate of 1 mm/min. The test temperature was consistent with that of SMP.

3. Theoretical analysis

3.1. Critical buckling analysis

The temperature influences whether the fibers in unidirectional fiber reinforced SMPC undergo micro buckling during bending. Liu et al.'s phase transition model of [27] explains that the interior of SMP consists of a glassy phase (frozen phase) and a rubbery phase (active phase) (as shown in Fig. 1). The total volume of SMP can be given in Eq. (1).

$$V = V_g + V_r \tag{1}$$

Where V is the total volume of SMP, V_g is the glassy phase volume, and V_r is the rubbery phase volume. The volume fraction of the two phases is stated as follows:

$$\phi_g(T) = \frac{V_g}{V},\ \phi_r(T) = \frac{V_r}{V} \tag{2}$$

Where $\phi_g(T)$ and $\phi_r(T)$ represent the volume fractions of the glassy and rubbery phases, respectively. The volume fraction of the glassy phase was calculated as Eq. (3) [28]. The relationship between the modulus of SMP and the volume fraction of the glassy state is expressed in Eq. (4) [24].

$$\phi_g(T) = \frac{1}{1 + \exp[g(T - T_r)]} \tag{3}$$

$$E_m(T) = (E_m(T_L) - E_m(T_H))\phi_g(T) + E_m(T_H) \tag{4}$$

Where T denotes the temperature of SMP, T_r denotes the reference temperature, and g denotes the parameter for adjusting the volume fraction with temperature change ratio. $E_m(T_L)$ and $E_m(T_H)$ are the

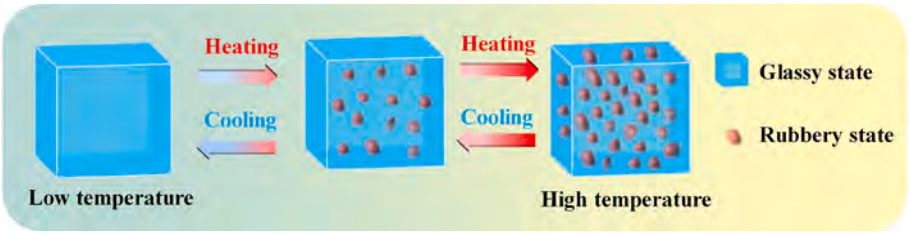

Fig. 1. Schematic diagram of mutual transition of the glass phase and the rubber phase.

moduli of SMP at low and high temperatures, respectively. The epoxy-based SMP was chosen as the research objective, with $E_m(T_L)$ and $E_m(T_H)$ values of 32 MPa and 2100 MPa, respectively. The DMA curve was fitted using Eq. (33), as shown in Fig. 2. The parameters g and T_r are determined to be 0.112 and 110 °C, respectively, using parameter fitting. As a result, the volume fraction of the glassy state can be calculated using the following equation:

$$\phi_g = \frac{1}{1+\exp[0.112(T-110)]} \tag{5}$$

Similar to Eq. (4), the change of Poisson's ratio of SMP with glass volume fraction is represented as [24]:

$$\nu_m(T) = \left(1-\phi_g(T)\right)\left(\nu_m(T_L)-\nu_m(T_H)\right)+\nu_m(T_L) \tag{6}$$

Where $\nu_m(T)$ is the Poisson's ratio of SMP related to temperature, $\nu_m(T_L)$ is the Poisson's ratio of SMP at low temperature, and $\nu_m(T_H)$ is the Poisson's ratio of SMP at high temperature. The Poisson's ratio of epoxy-based SMPs is considered to be 0.35 and 0.5 at low temperature and high temperature, respectively [24]. The shear modulus of the matrix can be written as:

$$G_m(T) = \frac{E_m(T)}{2(1+\nu_m(T))} \tag{7}$$

Where $G_m(T)$ and $E_m(T)$ denote the temperature-dependent matrix shear modulus and Young's modulus, respectively. SMPC exhibits large structural deformation and small strain when critical fiber buckling occurs. The following are the critical strain and critical curvature conditions for fiber buckling:

$$\varepsilon_{cb} = \frac{2\left(1-V_f\right)G_m(T)}{V_f E_f + V_m E_m(T)} \tag{8}$$

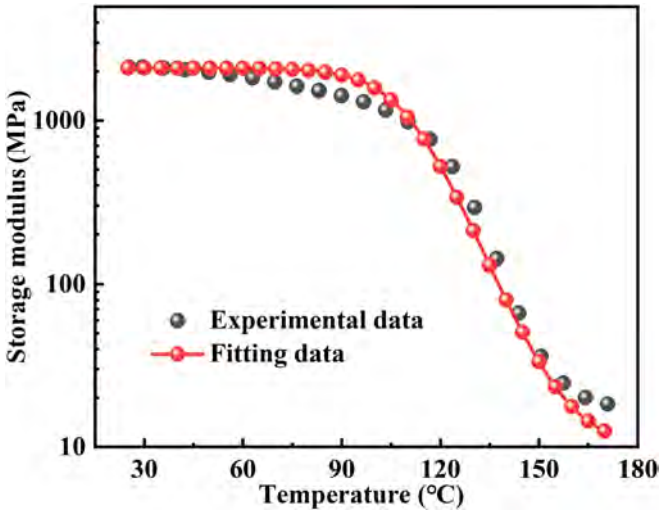

Fig. 2. DMA curve fitting of pure SMP.

$$\kappa_{cb} = \frac{4\left(1-V_f\right)G_m(T)}{t\left(V_f E_f + V_m E_m(T)\right)} \tag{9}$$

Where t denotes the thickness of SMPC. For unidirectional fiber-reinforced SMPC, the fiber will buckle when the compressive strain reaches a certain level. Whether the fiber buckles or not is determined by whether it breaks before reaching the bucking strain. The elongation at break of SMP under Tg is higher than that of the fiber. We simply need to evaluate whether the fiber will break before buckling. As a result, the fiber's critical buckling strain corresponds to its critical fracture strain, which represents the critical condition of fiber buckling, as follows:

$$\varepsilon_{cb} = \varepsilon_f \tag{10}$$

Where ε_{cb} and ε_f denote the critical buckling strain and critical fracture strain of fiber, respectively. Combining Eqs. (8) and (10) can assess if the fiber can buckle.

3.2. Strain energy and key parameters

After obtaining the critical buckling conditions of fibers during SMPC bending, the strain energy and key parameters of SMPC corresponding to the critical buckling were further investigated. When unidirectional fiber-reinforced SMPC bends around a cylinder at Tg, in-plane buckling occurs. The surface morphology and buckling deformation shape memory cycle of SMPC bending is shown in Fig. 3(a) and (b). The buckling morphology of fibers is wavy, and the adjacent fibers exhibit the same changing law. The cross section can be divided into buckling region, compressing-non buckling region and stretching region [26].

According to the principle of minimum energy, the shape of fiber buckling presents a sine/cosine wave, and the shape function of fiber buckling can be given as [29]:

$$y = \frac{2\lambda}{\pi}\sqrt{\kappa(z_{ns}-z)}\cos\left(\frac{\pi x}{\lambda}\right) \tag{11}$$

Where λ is the half-wavelength of fiber buckling, κ is the bending curvature of SMPC, z_{ns} is the neutral surface position, and x,y, z are spatial positions of the fiber. When the fiber buckles in plane, the buckling direction is solely in the X-Y plane. According to the shape function of the fiber, the shape of the fiber in the same plane is consistent. According to the stress analysis of the matrix between fibers, the primary deformation modes of the matrix in the X-Y plane are shear deformation and compression deformation in the X direction. Based on the equal strain assumption of the fiber and the shape function of the fiber, the shear stress of the matrix in the X-Y plane can be obtained using the variational principle [29]:

$$\tau_{xy} = -G_m(T)\sqrt{\kappa(z_{ns}-z)}\sin\left(\frac{\pi x}{\lambda}\right) \tag{12}$$

Where G_m and γ_{xy} represent the shear modulus and shear strain of the matrix in the X-Y plane, respectively. The amplitude of the fiber in the Z-direction is variable according to the shape function expression of the fiber. As a result, shear deformation occurs in the matrix between two adjacent fibers in the Y-Z plane, and the matrix's shear stress τ_{yz} can be

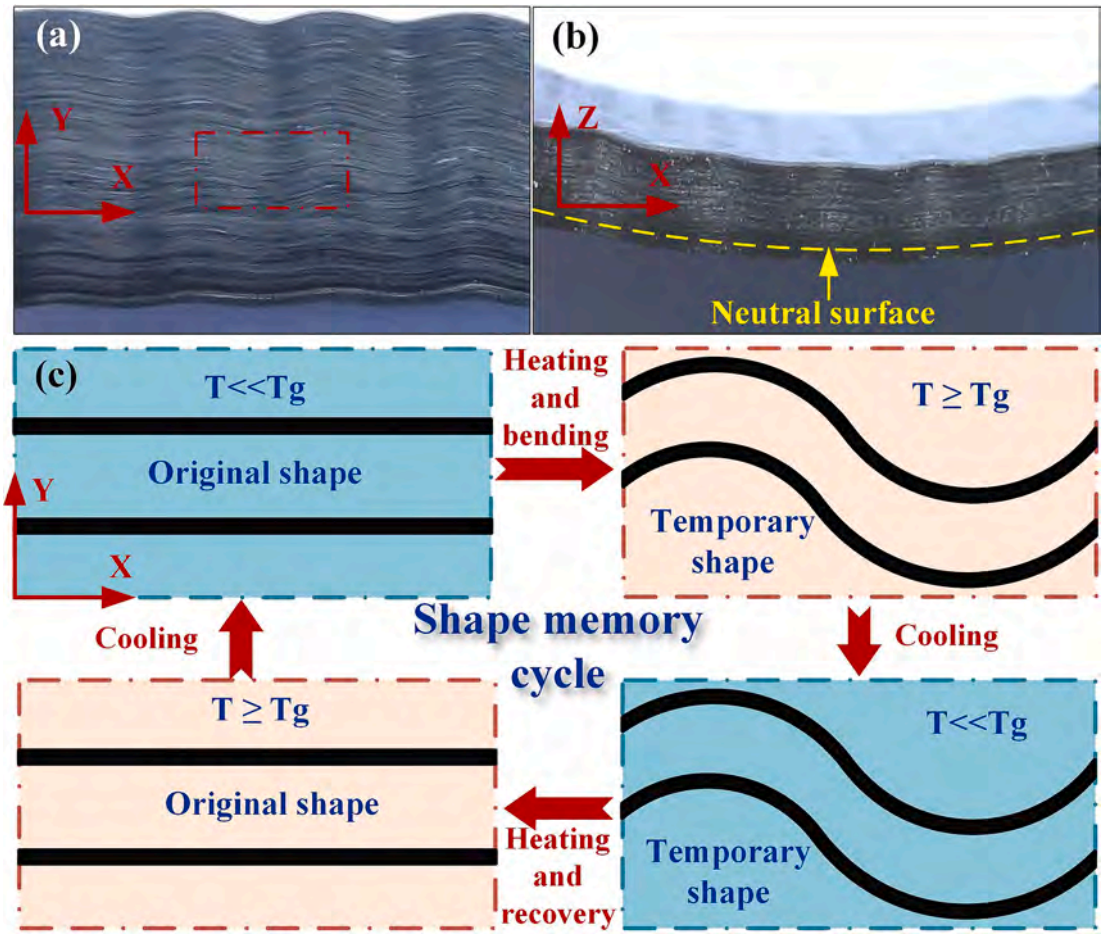

Fig. 3. Surface morphology and buckling deformation shape memory cycle of SMPC bending: (a) X-Y view; (b) X-Z view; (c) buckling deformation shape memory cycle.

written as:

$$\tau_{yz} = G_m(T)\frac{\delta y}{\delta z} = \frac{G_m \kappa \lambda}{\pi\sqrt{\kappa(z_{ns}-z)}}\cos\left(\frac{\pi x}{\lambda}\right) \tag{13}$$

Where γ_{yz} denotes the shear strain of the matrix in the Y-Z plane. According to the deformation analysis, the total strain energy can be expressed as:

$$U_T = U_{xx} + U_{xy} + U_{yz} + U_{fb} \tag{14}$$

Where U_T represents the total strain energy, U_{xx} represents the strain energy of the non-buckling region, U_{xy} and U_{yz} represent the shear strain energy of the matrix caused by γ_{xy} and γ_{yz}, respectively, and U_{fb} represents the strain energy of fiber buckling. The relevant derivation of Eqs. (15)–(22) can be found in our previous research [26,29]. The strain energy of the non-buckling region can be expressed as follows:

$$\begin{aligned} U_{xx} &= \frac{1}{2}\int_{z_{cb}}^{t}\int_0^b\int_0^l E(T)\varepsilon_{xx}^2 dxdydz \\ &= \frac{blE(T)\kappa^2}{6}\left[(t-z_{ns})^3 + (z_{ns}-z_{cb})^3\right] \end{aligned} \tag{15}$$

Where $E(T) = v_m(T)E_m(T) + v_f(T)E_f(T)$. The strain energy caused by shear strain γ_{xy} is obtained as follows:

$$\begin{aligned} U_{xy} &= \frac{1}{2}\int_0^{z_{cb}}\int_0^b\int_0^l \nu_m(T)G_m(T)\gamma_{xy}^2 dxdydz \\ &= \frac{bl\nu_m(T)G_m(T)\kappa}{2}\left[z_{ns}^2 - (z_{ns}-z_{cb})^2\right] \end{aligned} \tag{16}$$

The strain energy caused by shear strain γ_{xz} is given as follows:

$$\begin{aligned} U_{yz} &= \frac{1}{2}\int_0^{z_{cb}}\int_0^l\int_0^b \nu_m(T)G_m(T)\gamma_{yz}^2 dxdydz \\ &= \frac{bl\nu_m(T)G_m(T)\lambda(T)^2\kappa}{4\pi^2}\ln\left(\frac{z_{ns}}{z_{ns}-z_{cb}}\right) \end{aligned} \tag{17}$$

Because the in-plane buckling and out-of-plane buckling of SMPC during bending are only different in the direction of fiber buckling, their buckling shape function is the same. The buckling strain energy of fiber is:

$$U_{fb} = \frac{2bl\pi^2 E_f I_f \kappa}{d^2\lambda(T)^2}\left[z_{ns}^2 - (z_{ns}-z_{cb})^2\right] \tag{18}$$

Substituting Eqs. (15)–(18) into Eq. (14) gives the total strain energy of the in-plane buckling system:

$$\begin{aligned} U_T = {} & \frac{blE(T)\kappa^2}{6}\left[(t-z_{ns})^3 + (z_{ns}-z_{cb})^3\right] + \frac{blv_m(T)G_m(T)\kappa}{2}z_{cb}(2z_{ns}-z_{cb}) \\ & + \frac{bl\nu_m(T)G_m(T)\lambda(T)^2\kappa}{4\pi^2}\ln\left(\frac{z_{ns}}{z_{ns}-z_{cb}}\right) + \frac{2\pi blv_f E_f I_f \kappa}{\lambda(T)^2 d^2}z_{cb}(2z_{ns}-z_{cb}) \end{aligned} \tag{19}$$

When the compressing and non-buckling region is ignored, the strain energy of in-plane buckling system can be shown in Eq. (20).

$$U_T = \frac{blE(T)\kappa^2}{6}(t - z_{ns}(T))^3 + \frac{bl\nu_m(T)G_m(T)\kappa}{2}z_{ns}(T)^2 + \frac{bl\nu_m(T)G_m(T)\lambda(T)^2\kappa}{4\pi^2}\ln\left[\frac{4z_{ns}(T)\sqrt{v_f}}{d\sqrt{\pi}}\right] + \frac{2bl\pi v_f E_f I_f \kappa}{\lambda(T)^2 d^2}z_{ns}(T)^2 \quad (20)$$

Where $C = \nu_m G_m/(\nu_m E_m + \nu_f E_f)$. The expression of half-wavelength can be solved by using the minimum energy method, as shown in Eq. (21).

$$\lambda(T) = \left[\frac{8\pi^3 \nu_f E_f I_f\left(z_{ns}^2 - \frac{4C^2}{\kappa^2}\right)}{\nu_m(T)G_m(T)d^2\ln\left(\frac{z_{ns}\kappa}{2C}\right)}\right]^{\frac{1}{4}} \quad (21)$$

The amplitude of fiber buckling can be obtained by the relationship between fiber half-wavelength and amplitude.

$$A(T) = \frac{2\sqrt{\kappa(z_{ns} - z)}}{\pi}\left[\frac{8\pi^3 \nu_f E_f I_f\left(z_{ns}^2 - \frac{4C^2}{\kappa^2}\right)}{d^2\nu_m(T)G_m(T)\ln\left(\frac{z_{ns}\kappa}{2C}\right)}\right]^{\frac{1}{4}} \quad (22)$$

4. Results and discussion

4.1. Material properties

4.1.1. Dynamic mechanical properties

Fig. 4 show the DMA test curve of SMP and SMPC. The results reveal that the Tg of SMP was about 150 °C, while the Tg of unidirectional fiber-reinforced SMPC was 5 °C higher than that of SMP. The decreasing rate of the storage modulus of SMP gradually accelerates with increasing temperature and eventually becomes gentle. The modulus of storage modulus of SMPC has a small change at the beginning and increases after reaching a certain temperature, which is different from the trend of SMP. The incorporation of unidirectional fibers leads to a material whose modulus is less affected by temperature than that of pure SMP. This is because unidirectional fibers dominate the modulus of the composite, and the contribution of the polymer to the modulus is diminished. At room temperature (25 °C), the storage modulus of SMP and SMPC is about 2.1 GPa and 8.9 GPa, respectively. When the temperature reaches Tg, the storage modulus decreases to 32 MPa and 1.1 GPa, respectively.

4.1.2. Tensile and shear properties of SMP

The stress–strain curve of SMP at various temperatures is shown in Fig. 5(a). With increasing temperature, the fracture mode of SMP transitions from brittle to ductile with yield, and ultimately to elastic without yield. The stress–strain curves of SMP at room temperature and Tg exhibit almost linear elastic. At room temperature, the polymer was entirely in a glassy state, with the internal molecular chains frozen. At Tg, the polymer is in a rubbery state, with the internal molecular chains active. At temperatures of 60 °C, 90 °C, and 120 °C, the molecular chains within the material are only partially activated, resulting in a nonlinear stress–strain curve and yielding ductile fracture behavior.

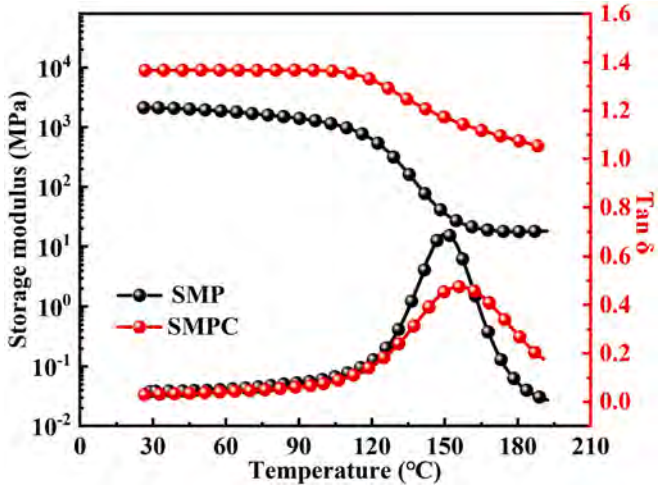

Fig. 4. DMA curve of SMP and SMPC.

Fig. 5(b) shows the strength and elongation at break of SMP at varying temperatures. The results indicate that the strength of the polymer decreased with the increase of temperature. This is because as the temperature increases, the mobility of the molecules within the polymer increases, which reduces the van der Waals forces that hold the molecules together. This increase in intermolecular mobility results in lower modulus and reduced ultimate stress [30]. The elongation at break of the polymer steadily rises with increasing temperature in the range of 25 ~ 120 °C. However, the elongation at break at Tg is lower than that at 120 °C, which is similar to the results reported in the literature [31]. It should be noted that different polymers may exhibit different behaviors. The tensile strength of pure polymer decreased from 57.1 MPa at room temperature to 8.2 MPa at Tg, while the elongation at break was about 10% and 40% at room temperature and Tg, respectively.

The shear test results of pure SMP at different temperatures are shown in Fig. 5 (c) and (d). The results show that the shear modulus and shear strength of pure SMP decrease with increasing temperature. The shear strength of pure polymer was approximately 40 MPa at ambient temperature and approximately 7.8 MPa at Tg, representing a decrease of nearly 80.5%. These results demonstrate the significant impact of temperature on the shear strength of the polymer. The elongation at break of the polymer was approximately 40% and 52% at room temperature and Tg, respectively. The ultimate shear strain of the pure polymer initially decreases and then increases with increasing temperature, consistent with the elongation at break of the polymer. This behavior is attributed to the similar mechanical properties exhibited by the interior molecular chains of the polymer under different deformation modes.

The shear fracture morphologies of pure SMP at 25 °C and 150 °C are shown in Fig. 5(e) and (f). At room temperature, the smooth surface of the pure polymer cracking was accompanied by almost straight cracks and a slight bifurcation at the ends of the cracks, indicating brittle fracture of SMP. In contrast, at 150 °C, the crack of SMP takes the shape of a rounded arc, indicating ductile fracture during crack extension at high temperatures. These observations are consistent with the pure SMP test curve, which demonstrates the ductile behavior of the polymer at elevated temperatures.4.1.3 Bending properties of SMPC.

Fig. 6(a) shows the three-point bending test curves of unidirectional fiber reinforced SMPC at various temperatures. The results indicate that the ultimate load of the material decreases as the temperature rises. When the temperature is less than 90 °C, the displacement-load curve is linear. However, when the temperature exceeds 120 °C, a linear curve is followed by a nonlinear curve. The stress–strain curve variation with temperature in this study is similar to the experimental results in the literature [32]. The load decreases when a certain displacement is reached. The displacement-load curve is linear because the fiber does not buckle and fracture immediately in the matrix with high modulus when the temperature is low. As the temperature rises, the modulus of the matrix decreases. When the bending strain reaches a specific threshold, the fiber buckles, and the curve becomes nonlinear. Upon loading the displacement to a certain extent, the material begins to deteriorate, and the load decreases. The critical buckling temperature of the composite can be determined by comparing the displacement-load curves at 90 °C and 120 °C.

The damage morphology of unidirectional fiber reinforced SMPC at room temperature and 150 °C is shown in Fig. 6(b) and (c). Combining Fig. 6(a) and (b), it is evident that brittle fracture occurred in the material at room temperature. The fracture morphology of the X-Z plane (cross section) clearly shows that the neutral surface position was

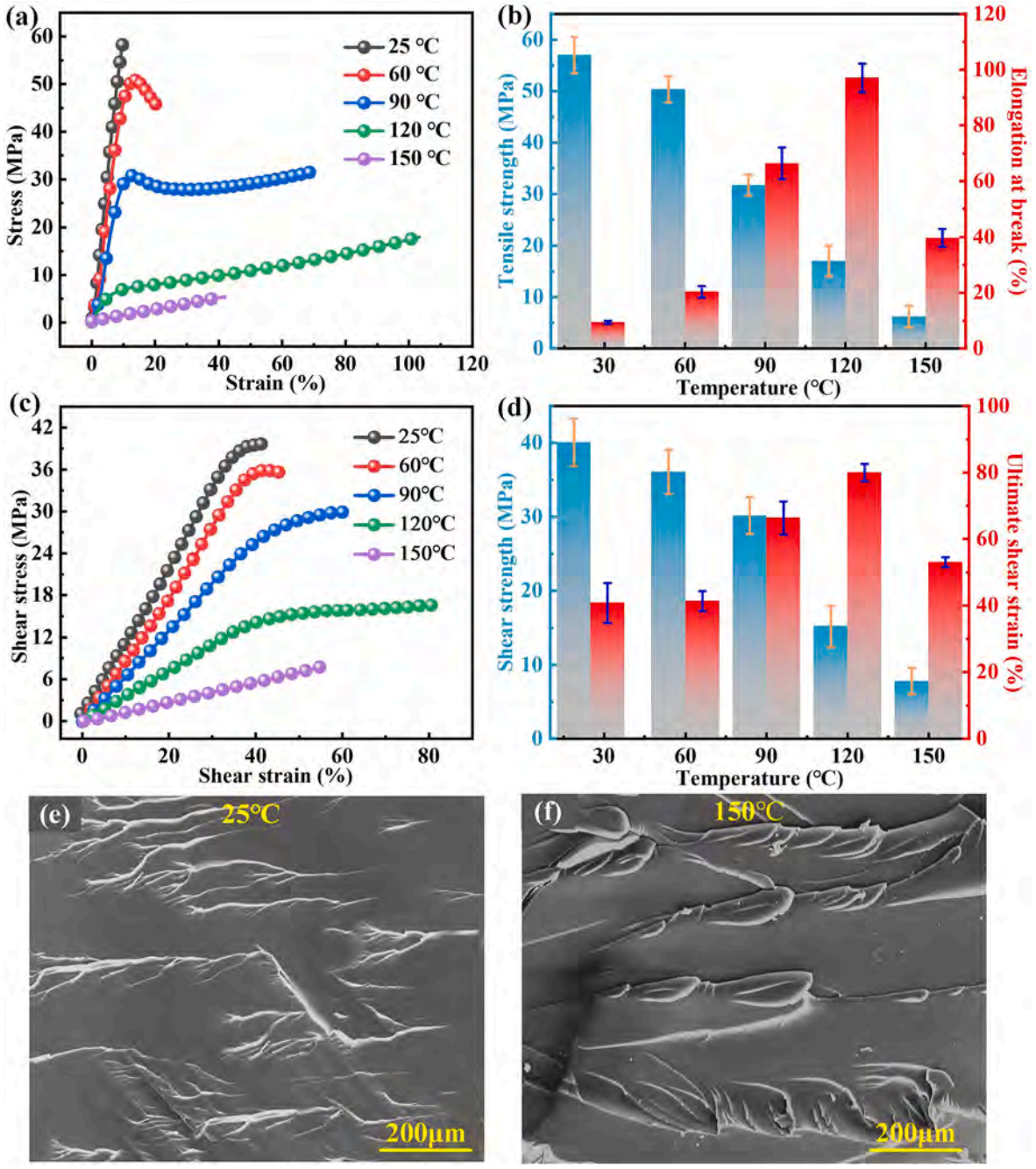

Fig. 5. Test results of pure SMP at different temperatures: (a) and (b) tensile test results; (c) and (d) shear test results; (e) and (f) shear fracture morphology.

roughly distributed in the middle of the cross section, indicating that the fiber does not buckle at this temperature. The material was damaged rather than broken when the temperature reached 150 °C. The fiber underwent buckling deformation from the damaged position in the X-Y plane. The matrix between the fibers simultaneously cracked, and the fiber fractured at the peak position of buckling due to the loss of the carrier of force transfer.

4.2. Critical bucking analysis

The tensile modulus and shear modulus of the shape memory matrix used in theoretical analysis at Tg are 32 MPa and 11 MPa, respectively. The size parameters of SMPC are 2 mm × 5 mm × 30 mm. According to Eq. (10), the condition for fiber buckling in SMPC is that the maximum compressive strain corresponding to critical buckling equals the fiber's fracture strain. At this point, the matrix is linear elastic (as shown in Fig. 5(a)). Therefore, when calculating the critical buckling of SMPC, both the matrix and fiber can be treated as linear elastic materials.

The effect of temperature and fiber volume content on the critical buckling curvature is shown in Fig. 7(a). The results reveal that the critical buckling curvature of fiber decreases with the increasing temperature, owing to a drop in matrix resistance to transverse deformation of fiber, rendering the fiber more susceptible to buckling. When the temperature rises from 25 °C to 170 °C, and the fiber volume content is 20%, the critical buckling curvature gradually decreases from 0.128 mm^{-1} to 8.2 × 10^{-4} mm^{-1}. Simultaneously, as the fiber volume content increases, so does the critical buckling curvature, making the fiber more prone to buckling. This is because the stiffness of the fiber's transverse deformation increases as the fiber volume content increases. When the composite is heated to 150 °C and the fiber volume content is increased

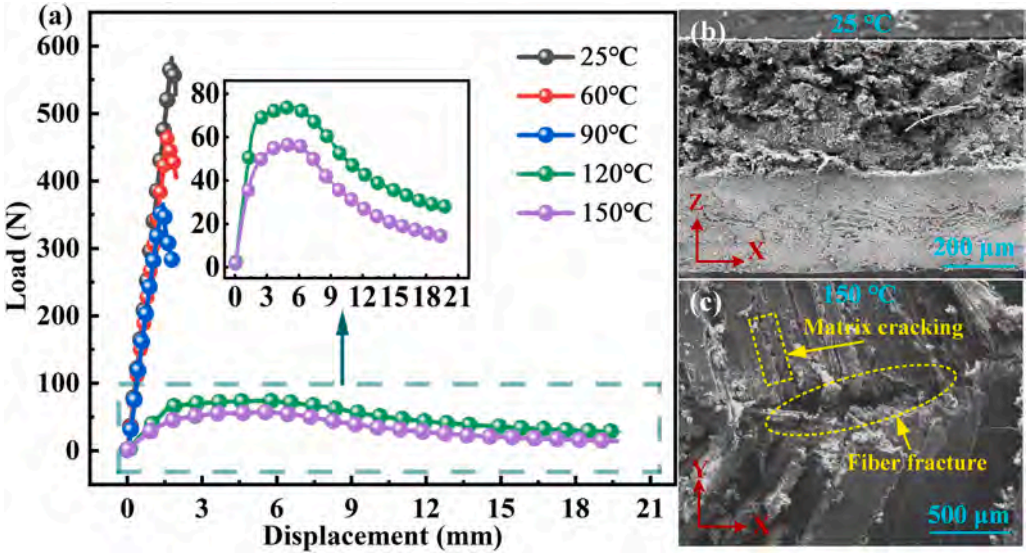

Fig. 6. (a) Bending properties of unidirectional fiber reinforced SMPCs at different temperatures; (b) Fracture damage morphology at 25 °C; (c) Fracture damage morphology at 150 °C.

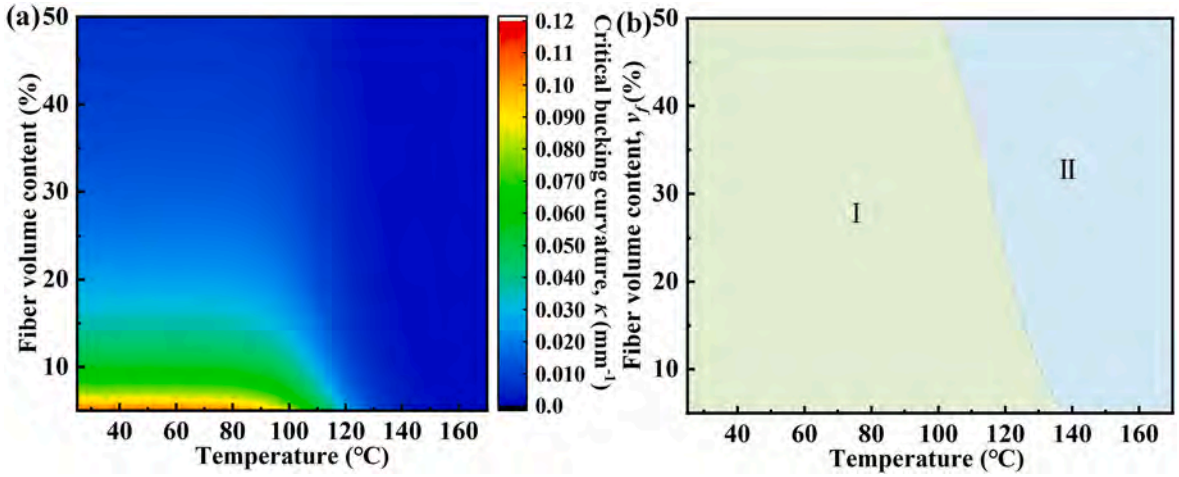

Fig. 7. (a) Variation of critical buckling curvature with temperature and fiber volume content ; (b)Effects of temperature and fiber content on fiber buckling: region I represents that the fiber cannot buckle when bending; region II represents that the fiber can buckle when bending.

from 5% to 50%, the critical buckling curvature decreases steadily from 3×10^{-3} mm^{-1} to 8.62×10^{-5} mm^{-1}.

Fig. 7(b) shows the effects of temperature and fiber volume content on fiber buckling. The fibers do not buckle and break directly when the temperature and fiber volume content are low (region I). The fiber buckles when the volume content and temperature of the fiber are in region II and the bending curvature reaches a certain value. The fiber volume content corresponding to critical buckling decreases with the rising temperature. Particularly, when the fiber volume content is 20%, 30% and 40%, the corresponding temperatures for critical buckling are 122 °C, 116 °C and 110 °C respectively.

To verify the correctness of the theoretical analysis, four-point bending tests was performed on unidirectional fiber-reinforced SMPCs. The prepreg process was used to prepare the SMPCs with a fiber volume content of 30% and dimensions of 120 mm × 5 mm × 2 mm. The temperature chamber provided a controlled environment for the test, with temperatures set at 120 °C, 130 °C, 140 °C, 150 °C and 160 °C. The critical buckling of the SMPC was determined by monitoring the changes in the load–displacement curve during the test. The bending modulus of the SMPCs shifts from linear to nonlinear when buckling occurs, and the loading is halted at this point while the displacement is maintained. Table 1 shows the theoretical and experimental results of the critical buckling curvature of unidirectional SMPCs at different temperatures. The theoretical and experimental results showed good agreement in terms of in order of magnitude, with the theoretical model's error being less than 20%. Considering the presence of defects in the test specimen and the limitations of the test method, this level of error is acceptable.

4.3. Key parameters analysis

Fig. 8(a) shows the temperature-dependent evolution of critical buckling curvature at various thicknesses ($V_f = 20\%$). The results reveal that as temperature rises, the critical buckling curvature decreases and the rate of decrease slows. Simultaneously, as the thickness increases, the critical buckling curvature decreases. With an increase in temperature, the difference in critical buckling curvature under different thicknesses diminishes. When the temperature is 150 ~ 170 °C, the critical buckling curvature of varied thickness is steady in 0 ~ 0.01 mm^{-1}. The thickness of SMPC does not affect the fiber buckling. Fig. 8 (b) shows the evolution of strain energy with the temperature at

Table 1
Theoretical and experimental values of critical buckling curvature under different temperatures.

Temperature (°C)		120	130	140	150	160
Bending radius of Critical buckling (mm)	Theoretical results	57.14	135.50	338.98	775.20	1219.52
	Experimental results	68.08 ± 6.22	152.56 ± 10.06	395.82 ± 15.26	839.96 ± 30.08	1357.36 ± 38.58
	Error	19.1%	12.5%	16.7%	8.3%	11.3%

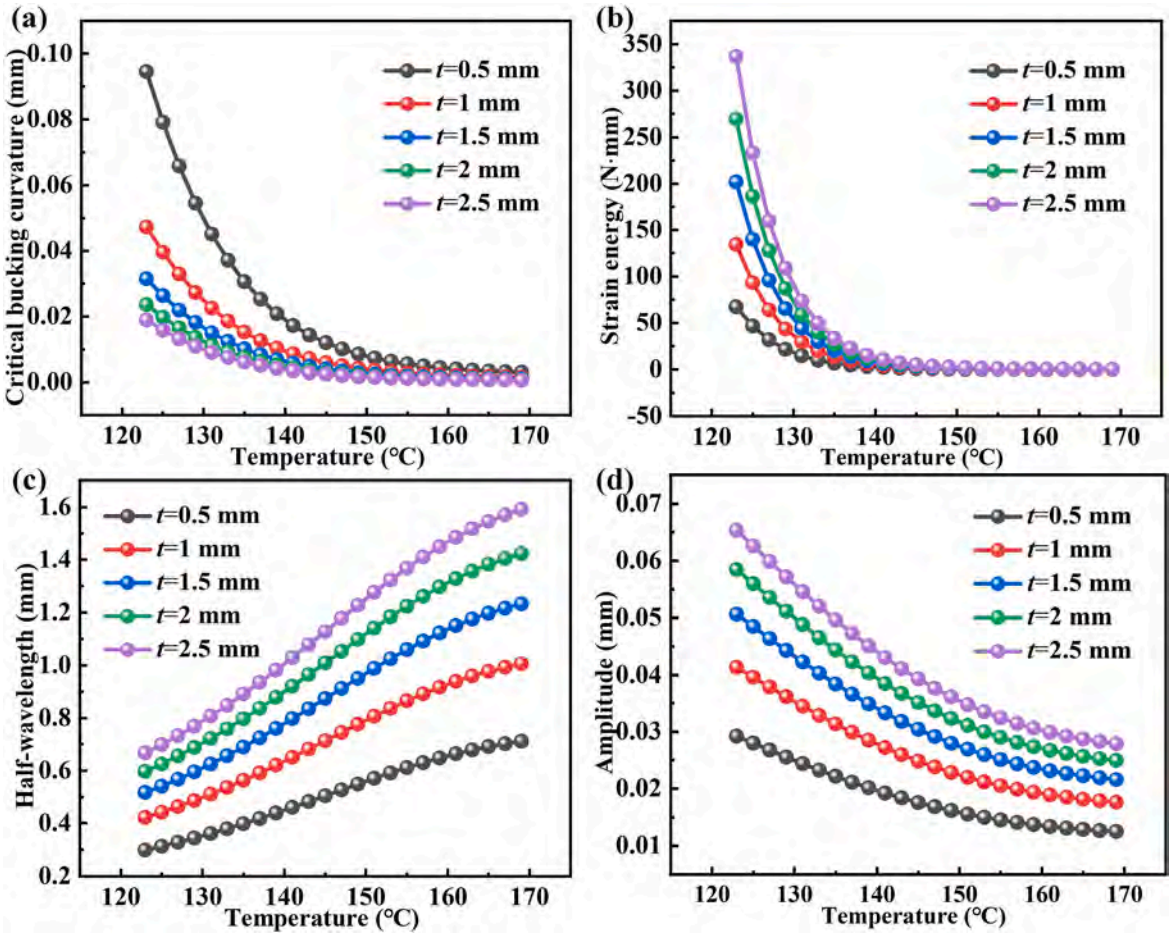

Fig. 8. Key parameters with respect to temperatures at different thickness: (a) critical bucking curvature; (b) strain energy; (c) half-wavelength; (d) amplitude.

different thicknesses. The results demonstrate that the strain energy decreases with rising temperature, and the rate of decrease gradually slows down. Additionally, as the thickness increases, the strain energy also increases. When the temperature is 150 ~ 170 °C, the strain energy varies slightly and approaches zero gradually.

Fig. 8(c) shows depicts the temperature-dependent evolution of the half-wavelength of critical buckling at different thicknesses. The results indicate that as the temperature increases, the half-wavelength exhibits an upward trend, with a fast initial growth rate that gradually slows down. The half-wavelength of critical buckling is close to the thickness of SMPC, and it is positively correlated with the thickness of SMPC. The evolution law of half-wavelength in this study is similar to that of triple SMPC in the literature [33]. Fig. 8(d) shows the evolution of critical buckling amplitude with the temperature at different thicknesses. The results indicate that the amplitude decreases with rising temperature, and the rate of reduction slows down. The amplitude of critical buckling is 1–2 orders of magnitude lower than the thickness of SMPC, indicating that the amplitude of critical buckling is very small. Simultaneously, the amplitude of fiber buckling is positively proportional to thickness.

Fig. 9(a) shows the temperature-dependent evolution of critical curvature at different fiber volume content (t = 2 mm). The results reveal that the critical buckling curvature decreases with an increase in fiber volume content, and the minimum temperature corresponding to critical buckling decreases progressively. It follows that the higher the fiber volume content is, the more prone buckling occurs. It can be concluded that the fiber volume content has a significant impact on the buckling behavior of the fiber. Fig. 9(b) shows the temperature-dependent evolution of critical buckling amplitude at various thicknesses. The findings demonstrate that the strain energy of critical buckling decreases as the temperature rises. This is due to the decrease in critical buckling curvature and matrix modulus with increasing temperature, resulting in a reduction of strain energy. Additionally, the strain energy corresponding to the lowest temperature increases as the fiber volume content increases. This is because a higher fiber volume content corresponds to a higher modulus of the matrix at the given temperature, leading to an increase in strain energy.

Fig. 9(c) depicts the evolution of half-wavelength of critical buckling at different fiber volume content. The results indicate that the half-wavelength of critical buckling increases with an increase in fiber volume content. This is due to the increase in section stiffness, which reduces the amplitude of fiber buckling while increasing the half-wavelength. Moreover, the half-wavelength corresponding to the

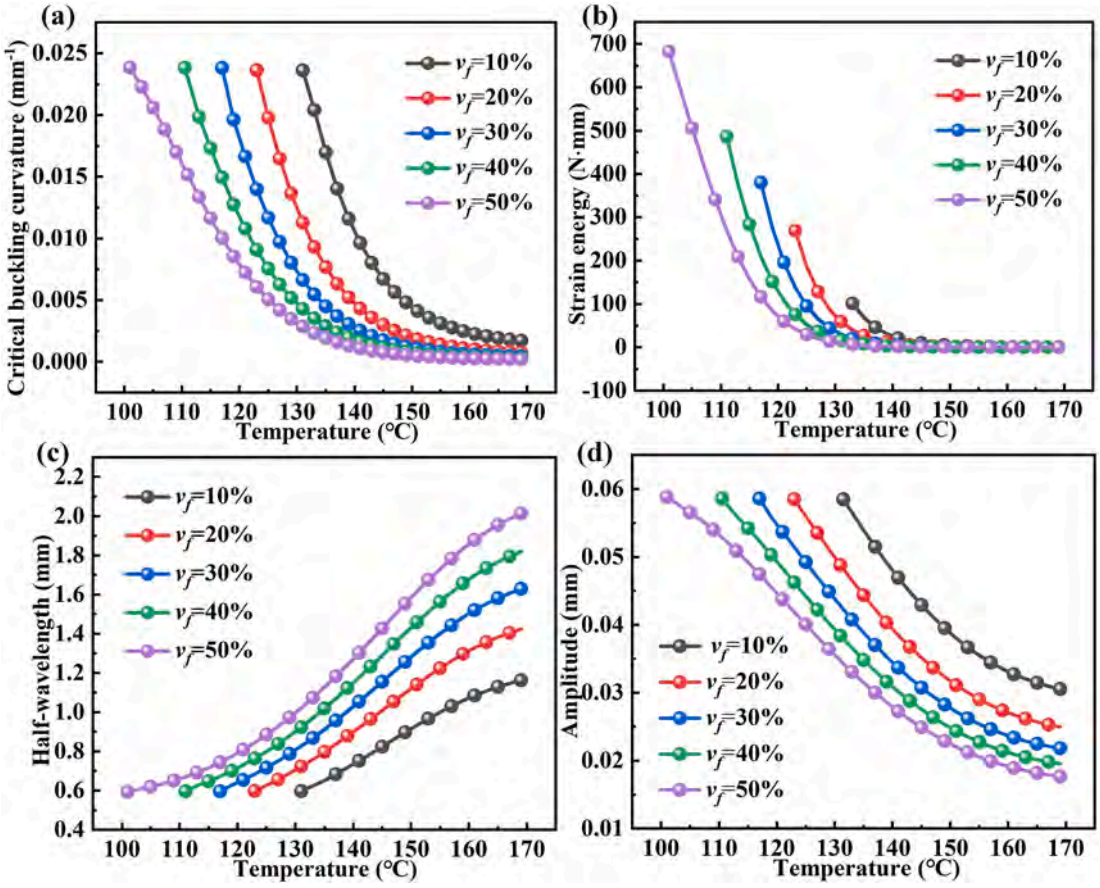

Fig. 9. Key parameters with respect to temperatures at different fiber volume content: (a) critical bucking curvature; (b) strain energy; (c) half-wavelength; (d) amplitude.

lowest temperature increases with an increase in fiber volume content, indicating that the fiber volume content has no effect on the half-wavelength of critical buckling at the lowest temperature. Fig. 9(d) shows the variation of the amplitude of critical buckling with the temperature at different fiber volume content. The findings demonstrate that an increase in fiber volume content leads to a decrease in the amplitude of critical buckling, and the amplitude of critical buckling at the lowest temperature remains constant.

The evolution law of critical bucking curvature, strain energy, half-wavelength, and amplitude with the thickness (T = 150 °C, V_f = 20%) is shown in Fig. 10(a). The results indicate that as the SMPC thickness increases (from 0.5 mm to 2.5 mm), the critical buckling curvature decreases (from 0.008 mm^{-1} to 0.0015 mm^{-1}), with a decreasing rate. Simultaneously, the strain energy, half-wavelength, and amplitude of critical buckling increase, with the rate of increase slowing down for half-wavelength and amplitude, while the strain energy of critical buckling grows linearly (from 0.35 N·mm to 2.24 N·mm).

Fig. 10(b) shows the evolution law of critical bucking curvature, strain energy, half-wavelength and amplitude with fiber volume content (T = 150 °C, V_f = 20%). The results show that as the fiber volume content increases (from 10% to 50%), the half-wavelength of critical buckling increases almost linearly from 0.91 N·mm to 1.58 N·mm. Meanwhile, the strain energy, half-wavelength, and amplitude of the critical buckling decrease, with the rate of decrease slowing down gradually.

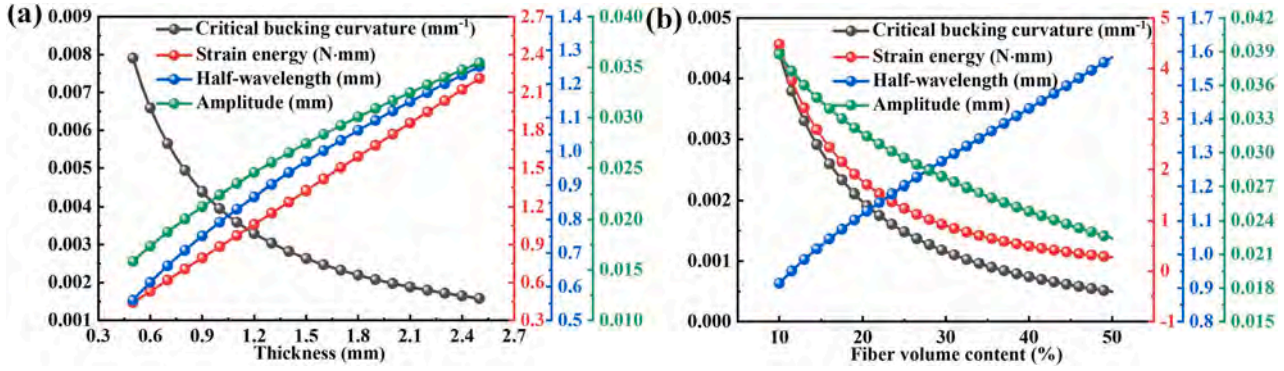

Fig. 10. Evolution of critical bucking curvature, strain energy, half-wavelength and amplitude: (a) with thickness; (b) with fiber volume content.

5. Conclusions

In this study, the effects of temperature on the mechanical properties and bending behaviors of SMPCs were investigated. Meanwhile, this work provided a simple and convenient model to predict the deformation behavior of SMPC with temperature. The primary conclusions are as follows:

a) The tensile strength and shear strength of SMP gradually rise with the increase of temperature, while elongation at break and ultimate shear strain initially increase and then decrease. SMPC is brittle fracture when it bends at low temperatures. SMPC does not break at high temperatures, but fiber buckling occurs, which allows it to withstand greater bending curvature.

b) The buckling behavior of SMPC is significantly influenced by temperature and fiber volume content. The higher the temperature and fiber volume content are, the easier the fiber buckling occurs. When the temperature of SMPC is below 102 °C, fiber buckling does not occur when the fiber content is less than 50%. The thickness of SMPC does not determine whether the fiber can buckle, but it does affect the critical curvature for fiber buckling.

c) The critical buckling curvature, strain energy, and amplitude exhibit an increase with rising temperature and fiber volume content. As thickness increases, the strain energy, half-wavelength, and amplitude also increase, while the critical buckling curvature decreases. The half-wavelength of critical buckling is in close proximity to the thickness of SMPC, whereas the amplitude of critical buckling is lower than the thickness of SMPC by 1–2 orders of magnitude.

This study did not take into account the viscoelasticity of SMPs, thus it cannot describe the shape memory behavior of SMPCs and the influence of loading rate on their bending performance. In the future, this material property can be considered to explore the shape memory behavior of SMPCs under temperature and loading rate changes.

Declaration of Competing Interest

The authors declare that they have no known competing financial interests or personal relationships that could have appeared to influence the work reported in this paper.

Data availability

Data will be made available on request.

Acknowledgements

This work is supported by the National Natural Science Foundation of China (Grant No. 11872020, 12272113).

References

[1] Lendlein A, Gould OE. Reprogrammable recovery and actuation behaviour of shape-memory polymers. Nat Rev Mater 2019;4(2):116–33.
[2] Chen H-M, Wang L, Zhou S-B. Recent progress in shape memory polymers for biomedical applications. Chin J Polym Sci 2018;36(8):905–17.
[3] Dayyoub T, Maksimkin AV, Filippova OV, Tcherdyntsev VV, Telyshev DV. Shape memory polymers as smart materials: A review. Polymers 2022;14(17):3511.
[4] Schauer S, Baumberg JJ, Hölscher H, Smoukov S. Tuning of structural colors like a chameleon enabled by shape-memory polymers. Macromol Rapid Commun 2018;39(21):1800518.
[5] Herath M, Epaarachchi J, Islam M, Fang L, Leng J. Light activated shape memory polymers and composites: A review. Eur Polym J 2020:136.
[6] Luo L, Zhang F, Leng J. Shape memory epoxy resin and its composites: from materials to applications. Research 2022;2022:9767830.
[7] Venkatesan H, Chen J, Liu H, Kim Y, Na S, Liu W, et al. Artificial spider silk is smart like natural one: having humidity-sensitive shape memory with superior recovery stress. Mater Chem Front 2019;3(11):2472–82.
[8] Guan X, Dong Y, Xia H, Yao J, Ni Q-Q. Mechanical and shape memory performance of shape memory polyurethane-based aligned nanofibers. Polym Test 2020;91:106778.
[9] Gu J, Zhao S, Zhang X, Cai Z, Sun H. A hygro-thermo-mechanical constitutive model for hygrothermally activated shape memory polymers under finite deformations. Mech Mater 2020;150:103594.
[10] Lee S-H, Kim S-W. Self-sensing-based deflection control of carbon fibre-reinforced polymer (CFRP)-based shape memory alloy hybrid composite beams. Compos Struct 2020;251:112544.
[11] Mattmann M, De Marco C, Briatico F, Tagliabue S, Colusso A, Chen XZ, et al. Thermoset shape memory polymer variable stiffness 4d robotic catheters. Adv Sci 2022;2103277.
[12] Luo L, Zhang F, Leng J. Multi-performance shape memory epoxy resins and their composites with narrow transition temperature range. Compos Sci Technol 2021;213.
[13] Garces IT, Ayranci C. Advances in additive manufacturing of shape memory polymer composites. Rapid Prototyp J 2021.
[14] Lei M, Chen Z, Lu H, Yu K. Recent progress in shape memory polymer composites: methods, properties, applications and prospects. Nanotechnol Rev 2019;8(1):327–51.
[15] Karger-Kocsis J, Kéki S. Review of progress in shape memory epoxies and their composites. Polymers 2018;10(1):34.
[16] Hung P-y, Lau KT, Guo Q, Jia B, Fox B, Materials N. Tailoring specific properties of polymer-based composites by using graphene and its associated compounds. Int J Smart Nano Mater 2020;11(2):173–89.
[17] Zhang J, Dui G, Liang X. Revisiting the micro-buckling of carbon fibers in elastic memory composite plates under pure bending. Int J Mech Sci 2018;136:339–48.
[18] Liu Z, Li Q, Bian W, Lan X, Liu Y, Leng J. Preliminary test and analysis of an ultralight lenticular tube based on shape memory polymer composites. Compos Struct 2019;223.
[19] Castro F, Westbrook KK, Hermiller J, Ahn DU, Ding Y, Qi H, et al. Time and temperature dependent recovery of epoxy-based shape memory polymers. J Eng Mater Technol 2011;133(2).
[20] Gu J, Zhang X, Duan H, Wan M, Sun H, Materials N. A hygro-thermo-mechanical constitutive model for shape memory polymers filled with nano-carbon powder. Int J Smart Nano Mater 2021;12(3):286–306.
[21] Yin C, Zeng H, Gu J, Xie Z, Sun H. Modeling the thermomechanical behaviors of particle reinforced shape memory polymer composites. Appl Phys A 2019;125:1–10.
[22] Bhola L, Mujumdar P, Guruprasad P. Thermo-mechanical analysis of shape memory polymer composite. Recent Advances in Computational Mechanics and Simulations: Volume-II: Nano to Macro 2021. p. 205–16.
[23] Li J, Liang Z, Chen K, Zhang X, Kang G, Kan Q. Thermo-mechanical deformation for thermo-induced shape memory polymers at equilibrium and non-equilibrium temperatures: Experiment and simulation. Polymer 2023;270:125762.
[24] Li F, Leng J, Liu Y, Remillat C, Scarpa F. Temperature dependence of elastic constants in unidirectional carbon fiber reinforced shape memory polymer composites. Mech Mater 2020;148.
[25] Wu X, Zheng H, Liu Y, Leng J. Thermomechanical property of epoxy shape memory polymers. Int J Mod Phys B 2010;24(15n16):2386–91.
[26] Liu ZX, Lan X, Liu LW, Bian WF, Liu YJ, Leng JS. Buckling behavior and damage mechanism analysis of fiber-reinforced shape memory polymer composites. Mech Mater 2022;175.
[27] Liu Y. Thermomechanical behavior of shape memory polymers. University of Colorado at Boulder; 2004.
[28] Su X, Peng X. A 3D finite strain viscoelastic constitutive model for thermally induced shape memory polymers based on energy decomposition. Int J Plast 2018;110:166–82.
[29] Lan X, Liu LW, Liu YJ, Leng JS, Du SY. Post microbuckling mechanics of fibre-reinforced shape-memory polymers undergoing flexure deformation. Mech Mater 2014;72:46–60.
[30] Plaseied A, Fatemi A. Strain rate and temperature effects on tensile properties and their representation in deformation modeling of vinyl ester polymer. Int J Polym Mater Po 2008;57(5):463–79.
[31] Du H, Liu L, Zhang F, Zhao W, Leng J, Liu Y. Thermal-mechanical behavior of styrene-based shape memory polymer tubes. Polym Test 2017;57:119–25.
[32] Zhang D, Liu L, Lan X, Li F, Liu Y, Leng J. Experimental study on nonlinearity of unidirectional carbon fibre-reinforced shape memory polymer composites. Compos Part A Appl Sci Manuf 2023;166.
[33] Tiwari N, Shaikh AA. Micro buckling of carbon fiber in triple shape memory polymer composites under bending in glass transition regions. Mater Today 2021;44:4744–8.